# Elastic analysis of structural ensemble reveals the energetic basis of hand-over-hand in a AAA+ motor

Victor Hugo Mello
*Instituto Gulbenkian de Ciência, Oeiras, Portugal*

Jiri Wald
*Centre for Structural Systems Biology, Hamburg, Germany*

Thomas C Marlovits
*Centre for Structural Systems Biology, Hamburg, Germany*

Pablo Sartori
*Instituto Gulbenkian de Ciência, Oeiras, Portugal*
(Dated: October 4, 2024)

**Abstract.** Proteins carry out cellular functions by changing their structure among a few conformations, each characterized by a different energy level. Therefore, structural changes, energy transformations, and protein function are intimately related. Despite its central importance, this relationship remains elusive. For example, while many AAA+ assemblies are known to function using a hand-over-hand alternation of subunits, how energy transduction throughout the assembly structure drives hand-over-hand is not known. In this work, we unravel the energetic basis of hand-over-hand in a model AAA+ motor, RuvB. To do so, we develop a general method to compute the residue scale elastic energy due to structure changes and apply it to RuvB structures, recently resolved through cryo-EM. This allows us to quantify how progression through RuvB's mechanochemical cycle translates into residue scale energy transduction. In particular, we find that DNA binding is associated with overcoming a high energy barrier. This is possible through inter-subunit transmission of energy, and ultimately driven by binding of ATP. Furthermore, we show how this structure-inferred energetic quantification can be integrated into a non-equilibrium model of AAA+ assembly dynamics, consistent with single-molecule biophysics measurements. Overall, our work elucidates the energetic basis for the hand-over-hand mechanism in RuvB's cycle. Furthermore, it presents a generally applicable methodology for studying the energetics of conformational cycles in other proteins, allowing to quantitatively bridge data from structural biology and single-molecule biophysics.

PACS numbers:

## I. INTRODUCTION

AAA+ is a superfamily of protein assemblies that catalyze a wide range of cellular functions, ranging from protein degradation to DNA recombination. Despite this wide scope, AAA+ function is often based on the translocation of a polymeric substrate through the central pore of the assembly, typically hexameric [1]. Recent cryo-EM structures of several members of this superfamily have consistently shown that these assemblies adopt an asymmetric folding, in which individual subunits organise as a staircase around the translocated substrate [2–14]. Based on this structural insight, it was suggested that subunits occupying different positions relative to the substrate change conformation sequentially. In this so-called *hand-over-hand* mechanism, subunits alternate between substrate engaged and disengaged states, resembling hands pulling on a rope [1]. However, the underlying basis for such highly orchestrated motion across subunits remains unclear.

From a thermodynamic perspective, hand-over-hand coordination must arise from energy transduction. Energy transduction is fundamental to all molecular motors because it couples the energy released from a chemical cycle – ATP hydrolysis and nucleotide exchange – to the motion produced on a mechanical cycle – substrate translocation. Crucially, chemical energy is not only needed to sustain motion but also to ensure coordination of different components [15–19]. However, despite the central role of energy transduction in protein function [20–22], how this energy is distributed throughout the structure of proteins is largely unknown. Consequently, how to connect the energetics of protein function with detailed structural information remains an open question. This paper aims to characterize the energetic basis of the hand-over-hand mechanism in a AAA+ motor at the structural level, thus connecting structural biology with protein biophysics for this paradigmatic example.

To achieve this goal, we build on previous work [23, 24] and develop a general method by which conformational changes in the structure of a protein can be identified with residue scale changes in elastic energy (Fig. 1A and B). While elasticity was originally aimed to describe deformations in large objects, proteins have been shown to exhibit elastic behaviour [25–28]. Furthermore, deformations such as bending [29, 30], stretching [31], and twist-

ing [32] are routinely (yet informally) ascribed to protein structures. Here, we provide a method (see *Methods* for details) to locally quantify elastic energy from structural data, built on our recently published Protein Strain Analysis (PSA) python package [24]. Combined with knowledge of the chemical cycle, our method provides the basis for quantifying energy transduction for a molecular motor in its operational cycle, Fig. 1C.

We apply the method described above to study how energy transduction promotes hand-over-hand in RuvB, an AAA+ hexameric assembly. RuvB is a molecular motor that translocates DNA in the Holliday Junction, hence driving branch migration in bacteria, Fig. 1D. We base our analysis on RuvB structures engaged in its mechanochemical cycle, recently visualized by time-resolved cryo-EM [2]. We first show that a simple principle of minimal elastic deformation can sort the conformational cycle of RuvB, in agreement with the result of manual sorting. We then identify the spatial distribution of elastic energy along the conformational cycle, which reveals that attachment to the substrate, or DNA *hand in*, is associated with overcoming a large energy barrier. We show that the energy needed to overcome this barrier comes from nucleotide exchange, and is transmitted across assembly monomers. Finally, we integrate the structurally inferred energy landscape into a non-equilibrium kinetic model of RuvB hexamers, which recapitulates our findings and predicts assembly dynamics. Overall, our work provides the energetic basis for hand-over-hand in RuvB. More generally, our method can be used to connect structural variability with energetics in other proteins, particularly those for which a series of conformations are captured "in action" using time-resolved cryo-EM.

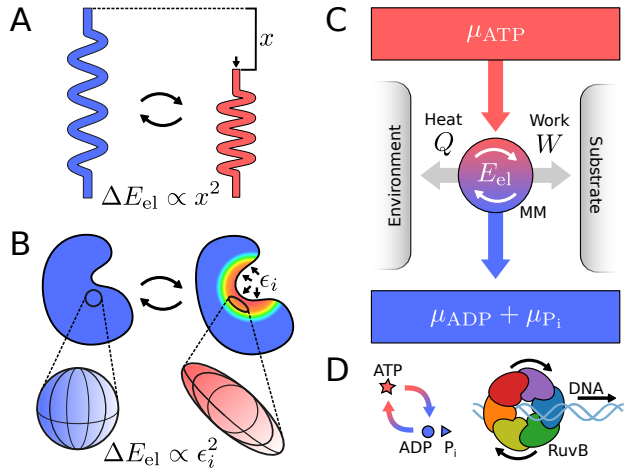


FIG. 1: *Elastic deformations mediate energy transduction.* **A.** The spring is the simplest example of an elastic system. Hooke's law establishes that when a relaxed spring is compressed by a length $x$, the change in elastic energy behaves as $\Delta E_{\rm el} \propto x^2$. **B.** For three-dimensional objects, like proteins, Hooke's law generalizes to continuum mechanics. A small region of a protein, depicted as a sphere in the reference conformation, deforms into an ellipsoid. This deformation is quantified by the local principal strains $\epsilon_i$ (with $i = 1, 2, 3$). The associated elastic energy change behaves as $\Delta E_{\rm el} \propto \epsilon_i^2$. **C.** Energy transduction in a molecular motor (MM) occurs when the difference in free-energy between ATP ($\mu_{\rm ATP}$), and ADP and $P_i$ ($\mu_{\rm ADP} + \mu_{\rm P_i}$) drives cyclic deformations in the motor ($E_{\rm el}$), resulting in work performance and heat release. **D.** RuvB is a hexameric AAA+ molecular motor which transduces chemical energy into motion of a DNA molecule through its central pore.

## II. RESULTS

**Cycle reconstruction using minimal deformation principle.** To describe energy transduction of a protein at the structural level it is necessary to resolve the multiple conformations it adopts along its mechanochemical cycle. These "structural snapshots" can be inferred, for example, from structural variability in the cryo-EM ensemble [33]. Once the conformations are obtained, a key task consists of finding their correct time order in the cycle, typically through visual inspection. Can an elasticity-based approach provide a systematic solution to this task?

For the case of RuvB, we consider five structures of the assembly ($s_1, \ldots, s_5$) and a putative reference not engaged on the cycle $s_0$, which were obtained and manually ordered in [2], Fig. 2A and *Methods*. Upon the completion of one cycle, each of the RuvB subunits switches to the next position relative to the DNA molecule. Altogether, the five cycle hexamers and the position switching rule imply that RuvB subunits perform a cycle with 30 conformations, Fig. 2B. From now on, we refer to each of these conformations by a letter, indicating a position relative to the DNA, and a number, indicating the numbering of the structure, e.g., F1, F2, ..., A5. Crucially, ordering the five structural snapshots as done in [2] involved extensive and time-consuming geometrical analysis, visual inspection, and careful evaluation of nucleotide-binding sites' electronic densities. We now provide an alternative approach for time ordering based on protein elasticity.

Specifically, we use a principle of minimal elastic deformation, by which subsequent structures in the cycle correspond to the smallest deformations, see *Methods* and *SI* Fig. 9. First, we calculate the residue-scale strain tensor –a quantity foundational to elasticity theory that measures local deformation [34]– over all possible pairs of conformations. Second, from this tensor we extract the local principal strain $\epsilon_3$, compute its average over all residues, and construct a matrix of size $30 \times 30$ with all pairwise comparisons (see *SI* Fig. 10 for an analysis including $s_0$). Pairs of conformations to which correspond a large matrix element are very different, as they relate to each other by a large deformation. Third, to interpret the matrix of deformations, we project it in two dimensions using Multidimensional Scaling (MDS)

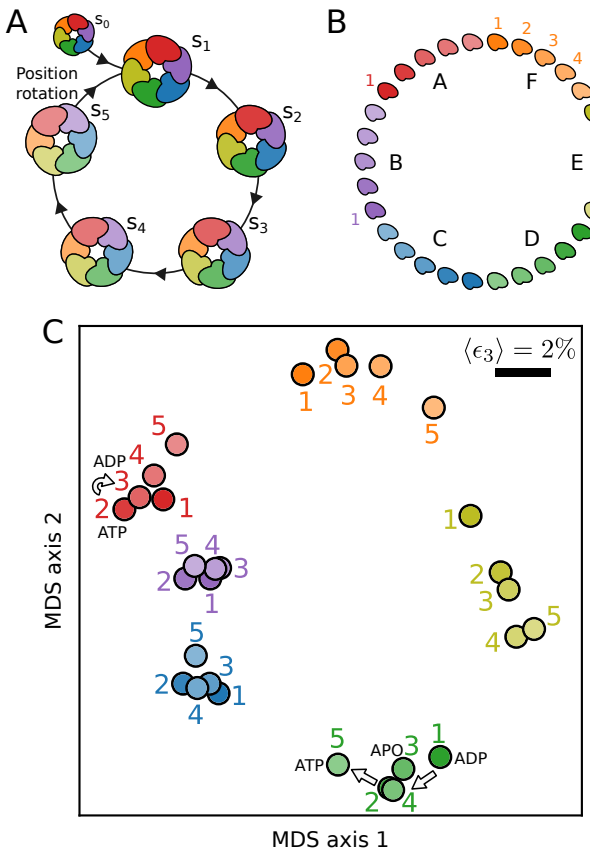


FIG. 2: *Minimal deformation principle reconstructs RuvB monomer cycle.* **A.** Sketch of RuvB hexameric cycle (states $s_1, \ldots, s_5$) together with the initial state ($s_0$). In the final transition, $s_5 \rightarrow s_1$, subunits switch to the next position (counterclockwise). **B.** The ordered assembly states together with the position switching rule imply that each RuvB subunit undergoes a cycle of 30 conformations. **C.** Low-dimensional embedding of pairwise comparisons between RuvB subunits is arranged in a cycle. Conformations cluster according to their position and a parsimonious order from 1 to 5 can be deduced for positions F, A, E and D. We use Multidimensional Scaling on the mean strain values, $\langle\epsilon_3\rangle$, for each pairwise comparison. The length of the scale bar indicates a mean strain of 2% for both axes. The plot depicts the mean of 100 individual MDS realizations.

[35, 36]. The resulting projection shows that subunits cluster in agreement with their position in the assembly (different colors), Fig. 2C. Furthermore, within these clusters, we can identify the order of the cycle substeps (1 to 5), which corresponds to the temporal order of the hexameric assemblies. Overall, our unbiased approach independently validates the ordering of structural snapshots in the mechanochemical cycle of RuvB.

**Elastic energy of the mechanochemical cycle at the subunit and residue scales.** Having shown the importance of elasticity in recovering the RuvB cycle, we now compute the elastic energy of all thirty conformations. To do so, we use as reference an assembly structure, $s_0$, that is not engaged in the mechanochemical cycle [2] and compute the elastic energy of each subunit compared to the reference, see *Methods* for details. Figure 3A shows the magnitude of elastic energy as a heat map on each conformation. We find that the spatial distribution of elastic energy is highly heterogeneous, with small regions accumulating most of the energy. Additionally, this distribution exhibits significant variation across different conformations (*SI* Fig. 11). We now quantitatively analyze these energetic patterns.

To obtain a global view of RuvB energetics we compute the total elastic energy per subunit, Fig. 3B. The resulting energy landscape is smooth and consists of a steady build-up of an energetic barrier in DNA free states and a decrease to a flat landscape in DNA bound states. Note that the highly energetic conformations (D, E and F) correspond to the "converter module" hypothesised in [2] to mediate energy transduction. At a local scale, we describe the elastic energy for each residue by a trajectory over conformations, Fig. 3C. These trajectories show that different residues are more deformed in specific moments of the mechanochemical cycle. We identify four mechanically active regions based on the variability of the energy trajectories, Fig. 3D and E (see *Methods*). Interestingly, all four regions are discontinuous in sequence but perform similar interaction patterns (*SI* Fig. 12 and Movies 1-4), suggesting that despite containing relatively distant residues, each region is consistently related to the same function.

Region 1 comprises part of the nucleotide-binding pocket and connects small and large ATPase domains. Region 2 localises mostly to sensor 1, a loop motif conserved in all AAA+ [37] whose specific role is critical for function but not consensual [1, 38–40]. Region 3 belongs to the head domain (C-terminal), which interacts with the DNA substrate. Region 4 largely coincides with a conserved structural motif named pre-sensor I $\beta$-hairpin, an insertion common to PS1 clade of the AAA+ superfamily, crucial for function [41]. In the context of RuvB, this motif provides direct and transient protein-protein interactions between RuvB and RuvA [42].

To summarise, we have identified the energy landscape of RuvB and key mechanically active regions in the structure. In the following, we study energy transduction through these regions and its connection to hand-over-hand. To this end, we analyse energetic exchanges with the DNA substrate (region 3, related to translocation), across RuvB subunits (regions 2 and 3, related to inter-subunit coupling), and with the nucleotide (region 1, related to chemical driving). Deformations in region 4 relate to the dynamic interactions with RuvA, therefore playing a role in the assembly cohesion, which is outside the scope of this paper. Altogether, these elements compose the energetic contributions for the function of a molecular motor, Fig. 1C.

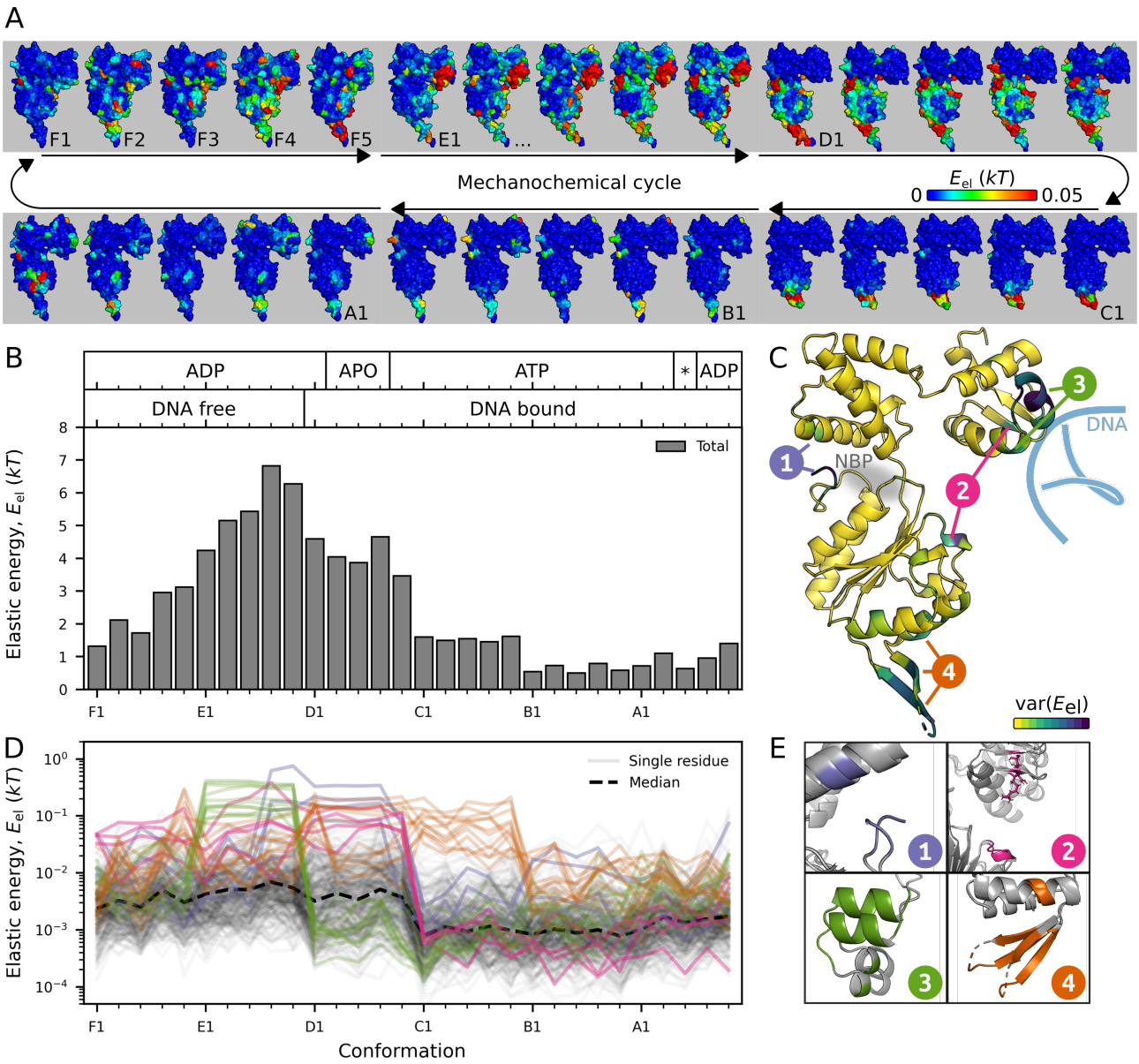


FIG. 3: *Elastic energy content of a RuvB subunit along its mechanochemical cycle.* **A.** We calculate the elastic energy content in the RuvB's protein structure at a residue level for its conformational cycle in units of $kT$, with $k$ the Boltzmann constant and $T$ the temperature. **B.** The sum of all elastic energy is represented throughout the cycle, representing RuvB's energy landscape. On top, the conformations are labelled according to their nucleotide content and engagement or not with the substrate. **C.** Elastic energy trajectories of each residue throughout the conformational cycle. The top 10% residues with most energetic variability display different characteristic trends of elastic energy trajectories, which led us to identify the mechanically active regions, shown in different colors. **D.** RuvB subunit (A1 conformation in the figure) color-coded with the variance of elastic energy across conformations. The most variable residues, grouped into four mechanically active regions, are marked by dark blue colors. Note that region 1 localises close to the nucleotide-binding pocket, and region 3 localises close to the DNA molecule. **E.** The structure of the four regions is displayed in two conformations with different energy contents. The regions are numbered and colored consistently throughout the manuscript.

**Energy is released upon transition to DNA-bound state.** A central aspect of molecular motor energetics is that they perform mechanical work by moving relative to a substrate [25]. For some AAA+, the motion of the substrate throughout the pore arises from a sequential hand-over-hand action of the different subunits [1], as is apparent by the staircase arrangement of the subunits around DNA, Fig. 4A. To quantify the energetics of this translocation process, we identify all the residues in RuvB that establish polar interactions with DNA across

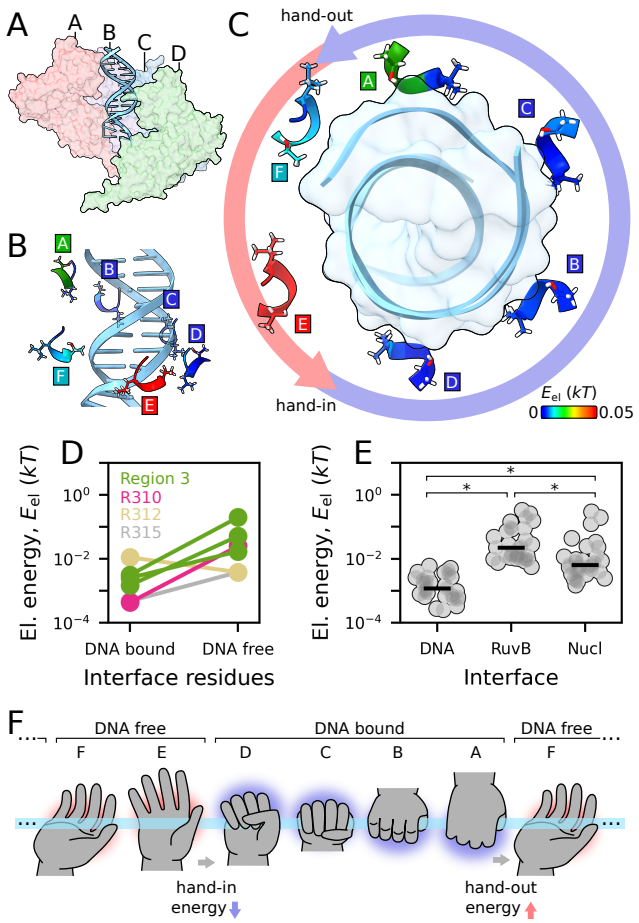


FIG. 4: *Energetics of the RuvB/DNA interface.* **A.** Global view of the RuvB subunits A, B, C and D arranged as a staircase around the DNA (assembly state $s_5$). **B/C.** Residues G279-T282, belonging to region 3, colored by elastic energy (side view in B and top view in C). **D.** Mean elastic energy content of residues in DNA bound and DNA free states. Except for R312, all residues display higher elastic energy when not interacting with the DNA, which corresponds mostly to positions F and E. **E.** Total elastic energy of different interfaces, with each data point corresponding to a conformation. RuvB/DNA interface is less energetic than RuvB/RuvB and RuvB/Nucleotide interfaces throughout the mechanochemical cycle (Kruskall-Wallis test $p < 0.05$; Mann-Whitney U test, $p < 0.05$, Bonferroni corrected). **F.** Sketch representing "hand-over-hand" with the energy content of RuvB/DNA interface appearing as a red (high energy) or blue (low energy) glow. Each hand represents the same RuvB subunit progressing over time through its conformational cycle (from left to right). For visual clarity, only six of the thirty conformations are shown.

each conformation, (see *Methods* for the procedure and *SI* Fig. 13 for all polar interactions). The RuvB/DNA interface is highly dynamic and comprises six residues, some of which belong to regions 2 and 3. Because most of these interactions are established in conformation D1 and are lost in conformation A5, we name *hand-in* the transition E→D, and *hand-out* the transition A→F.

Figures 4B and C show the energy content of region 3 residues in the RuvB/DNA interface. Remarkably, we find that these residues interact with DNA when they are in a low energy state, colored in blue (see also *SI* Fig. 14). Conversely, they exhibit high elastic energy when they do not interact with the DNA, Fig. 4D. When compared to other interactions, such as with the nucleotide and across RuvB subunits, interactions with DNA are characterized by a low elastic energy, Fig. 4E. Overall, this shows that after DNA hand-out the interface accumulates elastic energy that is then released upon DNA hand-in. Therefore, DNA stabilizes the interface, see Fig. 4F for schematics. Next, we investigate how inter-subunit interactions plays a role in transmitting energy to this interface during the DNA free conformations, i.e. between *hand-out* and *hand-in*.

**Inter-subunit coupling drives DNA hand-in.** Above, we showed that in DNA free states RuvB increases its energy, i.e., it climbs an energy barrier. How can these energetically unfavourable dynamics unfold? To address this question, we now investigate energy transduction across neighbouring RuvB subunits by characterising their interface. As shown in Fig. 5A, we define the forward subunit (pink) as the subunit forward to the interface according to the cycle orientation, and correspondingly for the backward subunit (gray). We find that regions 2 and 4 dominate the elastic energy at the forward subunit (Fig 5B), whereas region 3 accounts for most of the elastic energy at the backward subunit (Fig 5C). In particular, elastic energy is high when the forward subunit is in the DNA bound position D and the backward subunit in the DNA free position E. Therefore, the interface between subunits D/E has increased elastic energy on both sides.

We now focus on the interaction between regions 2 and 3, which come in contact with each other from opposite sides of the interface throughout the cycle (Fig. 5D-F, and *SI* Fig. 12 for the complete interaction profile). From the inspection of these regions at a molecular level, we observe two noticeable patterns: *(i)* in region 3 at the backward subunit, the highly energetic states correspond only to conformation D1 to D5, where a large displacement of the whole head domain is observed; and *(ii)* in region 2 at the forward subunit, the increase and decrease of elastic energies correlate with switches in the secondary structure from a loop (high elastic energy, F1 to D5) to a $3_{10}$ helix conformation (low elastic energy, C1 to A5), see *SI* Fig. 15. Note that $3_{10}$ helices are sterically unfavourable [43, 44], so that their structure can be involved in energy storage. In summary, these deformation patterns indicate that energy storage and release in region 2 resemble a spring-like mechanism, by which one subunit assists the displacement and repositioning of its neighbour. Such rearrangement accommodates RuvB within the double-helix minor groove, a contact that establishes the basis of hand-in for RuvB, see Fig. 5G.

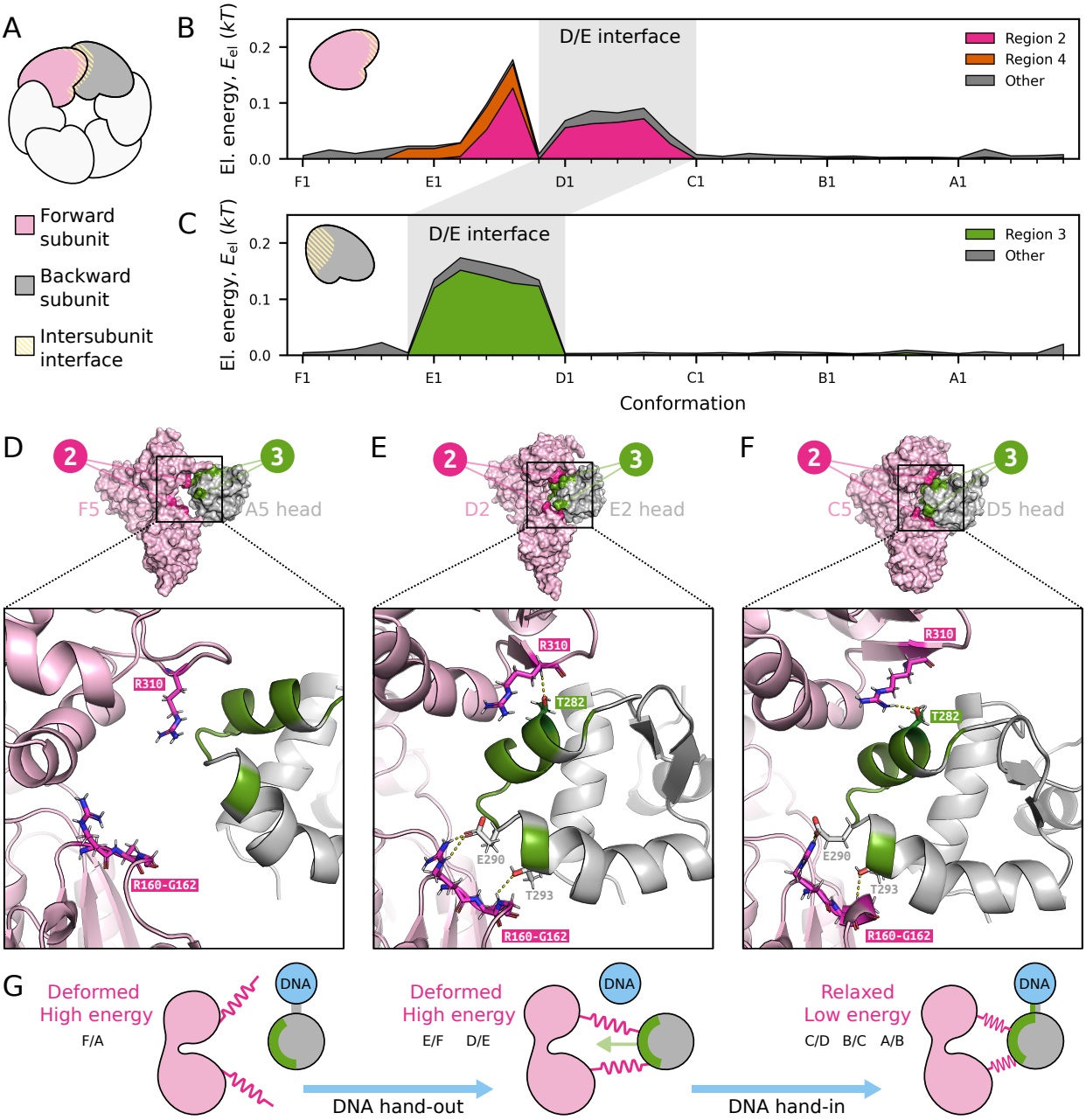


FIG. 5: *Energy transduction across adjacent RuvB subunits.* **A.** Schematic of the interface between the forward and the backward subunits. The nomenclature *backward* and *forward* refers to their order on the conformational cycle. **B/C.** Total elastic energy at the interface on the forward subunit (panel B) and backward subunit (panel C). Regions 2 and 4 represent a large fraction of the total elastic energy of the former and region 3 of the latter. **D/E/F.** Representative structures of the interaface dynamics: F5/A5 in panel D, where no interactions are found across subunits; D2/E2 in panel E, where these regions display polar interactions and residues R160-G162 adopt a loop structure; and C5/D5 in panel F, where regions 2 and 3 interact, but R160-G162 adopt a $3_{10}$ helix structure. **G.** Schematic of the interaction and energy patterns between neighbouring RuvB monomers: forward subunit is in a high-energy state, it then approaches and binds the backward subunit, finally it releases energy as the backward subunit moves and binds to DNA.

**Nucleotide exchange is the energy source of the mechanochemical cycle.** So far we have shown that the mechanochemical cycle of RuvB is characterized by an energy build-up just before DNA hand-in, and that this build-up is associated with inter-subunit energy coupling. What is the ultimate source of this energy?

Following the framework in Fig. 1C, it is clear that

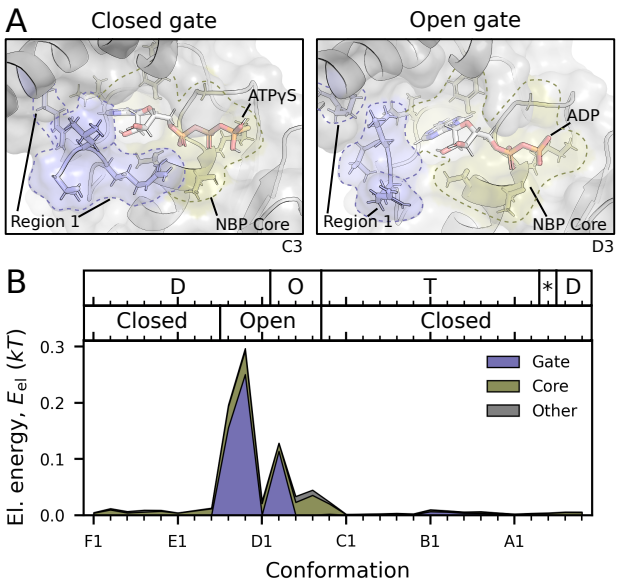


FIG. 6: *Nucleotide exchange drives hand-over-hand.* **A.** Region 1, which surrounds the NBP, adopts two distinct conformations: closed, when the nucleotide is ATPγS (a slowly hydrolysable ATP analogue); and open, when the nucleotide is ADP. **B.** The elastic energy of residues interacting with the nucleotide is high and dominated by region 1 when this region adopts its open conformation. Top labels indicate nucleotide state in each conformation (D for ADP, O for empty, T for ATP, and * for ADP + $P_i$.

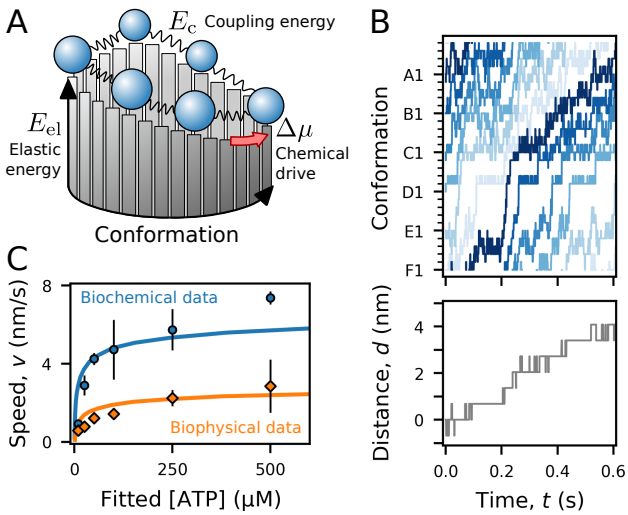


FIG. 7: *A kinetic model links protein energetics to protein dynamics.* **A.** Sketch of the kinetic model. The physical system comprises six subunits that populate conformations in a periodic mechanochemical cycle. Each conformation is associated with an elastic energy $E_{el}$ (bars on the vertical axis). Adjacent subunits interact through a coupling energy $E_c$ (represented by springs). Some transitions are biased in a particular direction (red arrow), with a chemical drive corresponding to the free energy from the nucleotide cycle $\Delta\mu$. **B.** Trajectories of RuvB conformations simulated with the model (top, subunits in shades of blue) and translocated distance of the DNA molecule (bottom, in gray). **C.** Speed-[ATP] curves from our simulations fitted with different experimental approaches (data points). We use single-molecule biophysics (orange) and biochemical branch-migration assays (blue) [45] to fit model parameters.

the source of energy is in the nucleotide cycle, and thus we turn our attention to the nucleotide binding pocket (NBP). The NBP is near region 1, identified in Fig. 3. This small region presents two different conformations, closed and open, acting as a gate, Fig. 6A. In the open conformation, both ADP release and ATP uptake take place; in the closed conformation, hydrolysis takes place.

We find that region 1 displays a high energy level while in the open conformation, when it also interacts with the nucleotide, see Fig 6B. In fact, in its open conformation region 1 accounts for 60% of the elastic energy of residues interacting with the nucleotide, largely surpassing the core of the NBP, which is mostly composed by the Walker A motif residues (see *SI* Fig. 16 for an analysis of Walker A and other conserved residues). In contrast, region 1 has low energy in its closed conformation.

This implies that the imbalance in chemical potential, which fuels RuvB dynamics, has a direct consequence on structural deformations during nucleotide exchange, but not hydrolysis. Furthermore, the open conformation of region 1 co-occurs with the conformations in which the interface between subunits is highly energetic, Fig. 5. Taken together, these facts show that the free energy of ADP binding is transduced across subunits to mediate the highly energetic hand-in interaction. This completes the energy transduction cycle behind hand-over-hand and substrate repositioning.

**Kinetic model of hand-over-hand links energetics to dynamics of RuvB assembly.** So far we have studied the energetic basis for the hand-over-hand mechanism of RuvB by analysing its structures. We now explore the implications of these results on the dynamics of the RuvB hexamer as a whole. To do so, we propose and implement a toy kinetic model that integrates the energetic analysis of structures performed above.

The dynamics of motor proteins can be modelled as stochastic transitions among a small set of states, see e.g. the classic works [20, 25, 46–48]. In the case of RuvB, an assembly state corresponds to each subunit adopting one of the 30 conformations described in Fig. 2B. The energetics of the model incorporates three central concepts discussed so far: elastic energy of each of the subunits, $E_{el}$; energy due to inter-subunit coupling, $E_c$; and free-energy exchange due to the nucleotide cycle, $\Delta\mu$ (Fig. 7A and *Methods* for mathematical formulation). Crucially, our model allows us to simulate the dynamics of an assembly quantitatively constrained by our previous energetic analysis of structures, Fig. 7B.

We calibrate the model to match the speed of translocation using data from RuvAB-mediated Holliday

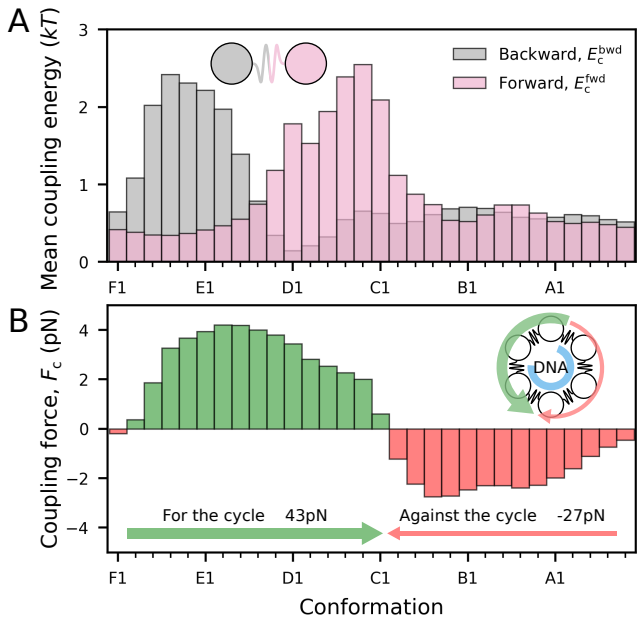


FIG. 8: *Coupling energy prediction of kinetic model.* **A.** Mean coupling energy at backward and forward interfaces (see schematic). The coupling energy is high before and after the elastic energy barrier. **B.** Total coupling forces, summed effect of the spatial derivative of backward and forward coupling energies. Bars in green represent forces aligned to the cycle direction (F → E) and in red, in the opposite direction (E → F). The model predicts a net positive force over the whole cycle. The cartoon represents the RuvB hexamer, with green and red curved arrows for the positive and negative forces, respectively.

Junction branch migration experiments [45]. In brief, by adjusting two free model parameters we are able to recapitulate the speed-[ATP] curves of single-molecule and bulk biochemical assays. Remarkably, our model shows good agreement with both assays by accounting for the extra drag due to the presence of a bead in the biophysical assay (Fig. 7C and *SI* Fig. 19 for details). Therefore, we have developed a model of RuvB hexamer dynamics that quantitatively bridges structural data of high spatial resolution to time-resolved single-molecule measurements.

**Simulated model trajectories recapitulate structural observations.** With the model parametrized, we can now computationally investigate the collective dynamics of the RuvB assembly. In particular, we focus on characterising the inter-subunit coupling in order to evaluate whether the model recapitulates our structural observations.

Our method inherently considers that adjacent subunits are allowed to transfer energy, but it does not set a priori the magnitude of this coupling at each conformation. To quantify the magnitude of the inter-subunit coupling throughout the cycle, we compute the coupling energy between adjacent subunits, see *SI:* Appendix H. Figure 8A shows that forward and backward coupling energy is localised in subunits before and after the peak in elastic energy. This supports that inter-subunit coupling is essential to support cycle progression, which is mainly hindered by a large energetic barrier in position E.

We then calculate the mean coupling force across subunits in each cycle conformation. The force, which corresponds to the derivative of the coupling energy (*SI:* Appendix H), determines the direction and intensity with which subunits push or pull each other. Figure 8B shows that the mean resulting force is positive (aligned to the cycle) in positions F, E, and D, and negative (opposed to the cycle) otherwise. Note that the assisting role of positive forces in crossing the energy barrier is reminiscent of the previously proposed role of the converter module [2, 49]. Overall, the emergent energy coupling landscape predicted by the model supports the idea that coupling is key in overcoming the hand-in energetic barrier.

## III. DISCUSSION

**Summary.** Protein function depends on structural deformations. Despite much of these deformations being caused by spontaneous thermal fluctuations, coordinated motion requires energy input [50]. This is particularly notable for motors, such as in the AAA+ superfamily, in which function is directly driven by the free-energy released from the nucleotide cycle. Despite this intimate relationship, protein energetics and function remain largely disconnected at the structural scale. In this work, we have linked these two aspects of proteins for a particular AAA+ assembly, RuvB. We have done so by following an interdisciplinary approach that combines elasticity-based data analysis of experimentally determined structures [23, 24, 51–55], and non-equilibrium thermodynamics modelling [20, 25, 46–48]. The key contributions of our work are twofold: a general methodology applicable to any ensemble of structures, and novel energetic insight into AAA+ hand-over-hand mechanism.

**Methodological considerations.** Our approach builds on the previously established Protein Strain Analysis [23, 24] and extends it with two new applications: first, unsupervised ordering of an ensemble of structures using strain as a dissimilarity metric; second, obtaining residue scale energetic information through an elastic description of protein structures. These applications are completely general and can be deployed to any protein for which multiple structures have been experimentally or computationally resolved.

Concerning the ordering of structural ensembles, there are related methods that investigate conformational variability. Examples are methods relying on Ensemble PCA or NMA [56–59], as well as methods aimed at heterogenous cryo-EM reconstructions [33, 60, 61]. Compared

to the first group, our approach analyses dissimilarities between pairs of structures, instead of structure-specific features such as atomic coordinates (for ensemble PCA) or their vibrational modes (for ensemble NMA). An additional difference is that PSA is independent of structural alignment, thus better characterizing motions between rigid domains [23, 24]. Compared to the second group, our approach presents the key difference that it relies on atomic maps, not raw EM micrographs. On the one hand, this makes PSA suitable to assess structures regardless of their acquisition approach (cryo-EM, X-ray diffraction, NMR, or computational structure prediction). On the other hand, our method is sensitive to the accuracy of the atomic-map reconstruction. A natural next step is to adapt the elastic approach to process raw experimental data. Overall, our method provides a readily interpretable low-dimensional representation of a set of structures.

Concerning energetics of protein structures, previous approaches have focused on the construction of energy landscapes from the raw ensemble of single-molecule cryo-EM images [60, 62–64] and molecular dynamics [65]. The key distinctive feature of our method is that it provides energetic information at the residue scale. To achieve this, we relied on a simple yet strong assumption: that the deformation of a protein relative to a reference state is well captured by a homogeneous and isotropic elastic model. While proteins have long been ascribed elastic properties [28, 66, 67], our model assumptions are a clear oversimplification. For example, proteins are generically anisotropic and non-homogeneous materials: proteins can be more easily deformed in specific regions from specific directions. One potential way to improve this is to use alternative methods, such as NMA [68] or $\beta-$factors from X-ray data to infer local elastic properties. Also, reference structures for deformations are likely pre-stressed [69], so that simple elastic energy expressions such as the one considered here may under or overestimate the energy of a deformed conformation. A potential way of addressing this is to consider plastic deformations in addition to the standard elasticity theory as a framework to model proteins [70].

**Relationship between mechanical and biochemical activity.** Our approach identifies few and small protein regions where deformations are large. A natural question is whether mechanically active regions are also likely to display specific biochemical functions.

In *SI* Fig. 16 we show that there is no clear relationship between high elastic energy and sequence conservation, which we use as a proxy for conservation of biochemical properties. In particular, in the mechanically active regions we find residues ranging from strongly conserved to not conserved at all. This might be due to a small overlap with biochemically active residues, which exhibit a large degree of conservation, whereas the remaining residues deform because they are contiguous in sequence. It is possible that this deformation has a mechanical role in transiently storing energy through deformation, and therefore does not require side chains with specific biochemical properties. Just as biochemical activity is associated with sequence conservation, it remains open whether mechanical activity is also associated with conserved structural features.

**Energetics of hand-over-hand in RuvB.** The hand-over-hand mechanism, commonly observed in AAA+ proteins, has recently been observed for RuvB [2]. In essence, hand-over-hand establishes that each subunit within the assembly sequentially alternates its conformation. After each DNA translocation step, each subunit adopts the conformation of its preceding neighbor. These conformations, characterized by their helical positioning relative to the DNA, play distinct roles in the DNA translocation process.

Our energetic analysis provides insights into these roles and how they interrelate. We found that the progression of the mechanochemical cycle is associated with overcoming an energy barrier during DNA-free conformations (F and E). Our findings suggest that mechanical coupling between subunits D and E plays a crucial role in assisting with the crossing of this barrier. Furthermore, we found that elastic deformations in the NBP during nucleotide exchange, rather than ATP hydrolysis, supply the energy that is transduced through inter-subunit coupling. This is in line with observations in other molecular motors, see [71–73]. In conclusion, an energetic cascade that starts in the NBP and is transmitted across chains leads to DNA hand-in, and constitutes the energetic basis of hand-over-hand in RuvB.

**From hand-over-hand to DNA translocation.** The relationship between hand-over-hand and substrate translocation for RuvB is still an open question. We propose a mechanism by which RuvB combines co-rotation with DNA and slippage along the DNA axis. This slippage allows DNA to displace along its axis while RuvB rotates at a fixed position relative to RuvA. We note that DNA slippage corresponds to DNA hand-out, which involves no changes in elastic energy of the corresponding subunit.

There are two key pieces of evidence supporting this view. First, it has recently been observed that nucleotide exchange and hydrolysis occur at fixed positions relative to RuvA [2], which is impossible without RuvB rotation. Second, single-molecule experiments have shown that the DNA molecule rotates when translocated by the RuvAB complex [45].

This mechanism suggests that RuvB can translocate the DNA through a restoring torque at the contact surface, which resists the direction of rotation. This aligns with the predictions of the kinetic model. In our analysis of coupling force (Fig. 8B), we found that subunits in C, B, and A display a coupling force that resists the hexamer rotation, even without the explicit mod-

elling of the DNA molecule. Altogether, this suggests that the subunits in these three positions are responsible for a gradual translocation of the DNA as they rotate.

**Alternative substrate translocation mechanisms.** We note that, while hand-over-hand is common among AAA+ proteins, it coexists with other translocation mechanisms [41]. For instance, the protease ClpXP shows evidence of both stochastic ATP hydrolysis and sequential bursts [74], while the bacterial pilus motors PilB and PilT-4 exhibit two-fold symmetric structures during their functional cycles [75]. Currently, no framework can explain or predict which translocation mechanism should be expected for a given AAA+. Clearly, many factors are at play, such as efficient energy usage, geometry of the translocated substrate, evolutionary contingency, and regulation. Nevertheless, the generality of our approach, which combines physics-based structural analysis with minimal mathematical modelling, paves the way to a systematic study of different mechanisms of AAA+ function.

## IV. METHODS

**A primer in Protein Strain Analysis.** To estimate the elastic energy associated with protein conformational changes, we first need to introduce strain, a well-established physical concept that quantifies deformation. In order to do so, we briefly describe the mathematical framework of elasticity theory. This method is explained in detail in [24] and implemented in the PSA python package available at `github.com/Sartori-Lab/PSA`.

Consider the three-dimensional coordinates of a given atom $i$ of a protein in two conformations, $\mathbf{x}_i$ and $\mathbf{X}_i$. A local deformation between these conformations is defined by the motion of the atom $i$ relative to its surrounding atoms, and it is quantified by the deformation gradient tensor $\mathbf{F}_i$. This matrix can be estimated using the atoms in a neighbourhood of the given atom $i$ as

$$\boldsymbol{\Delta}\mathbf{x}_i^j \approx \mathbf{F}_i \boldsymbol{\Delta}\mathbf{X}_i^j \quad , \tag{1}$$

where $j$ are all atoms in a local neighbourhood of $i$, and $\boldsymbol{\Delta}\mathbf{x}_i^j$ and $\boldsymbol{\Delta}\mathbf{X}_i^j$ are the displacement vectors between the atoms $i$ and $j$ in the different conformations. See *SI:* Appendices B and C for a formal definition of the neighbourhood used in this study. The above equation is typically over-determined, and we thus estimate $\mathbf{F}_i$ minimizing a quadratic error as proposed in [76], see also [24]. From the deformation gradient, we define the Lagrangian strain tensor $\mathbf{E}_i$, which captures the finite deformations around the atom $i$ regardless and has the advantage of being independent of structural alignment:

$$\mathbf{E}_i = \frac{1}{2}\left(\mathbf{F}_i^{\mathrm{T}}\mathbf{F}_i - \mathbf{I}\right) \quad . \tag{2}$$

The strain tensor can be viewed as compressions or expansions in three orthogonal directions. This is represented schematically in Fig. 1B by the deformations that transform a sphere into an ellipsoid. Associated to this view we define the three principal strains $\epsilon_{i,a}$, with $a = 1, 2, 3$, the eigenvalues of the strain tensor given by $\mathbf{E}_i\mathbf{v}_{i,a} = \epsilon_{i,a}\mathbf{v}_{i,a}$, where the eigenvectors $\mathbf{v}_{i,a}$ are the directions of each principal strain. The principal strains are ordered as $\epsilon_{i,1} < \epsilon_{i,2} < \epsilon_{i,3}$.

**Elastic energy from protein structures.** In order to discuss protein energetics we use a hyperelastic model for the Helmholtz free-energy density, $\Psi(\mathbf{E})$ [77]. Specifically, we use a Saint Venant-Kirchhoff model for which $\Psi$ is given by:

$$\Psi(\mathbf{E}_i) = \frac{\lambda}{2}\mathrm{tr}(\mathbf{E}_i)^2 + \mu\mathrm{tr}(\mathbf{E}_i^2), \tag{3}$$

where $\lambda$ and $\mu$ are the first and second Lamé constants, respectively. The advantage of using this form of $\Psi$ is that $\lambda$ and $\mu$ relate to the Young modulus, which has been measured experimentally and estimated computationally for proteins [25, 66, 67, 78–80]. This is not the case for most hyperelastic models. Also, this form of $\Psi$ is a strictly non-negative function, unlike other simple elastic models that might yield negative energies for compressed regions.

Because energy is an extensive quantity, it is defined as the integral of the energy density over the protein's volume. We compute the elastic energy $E_{\mathrm{el}}$ contained in the deformations of the neighbourhood of an atom as

$$\begin{aligned} E_{\mathrm{el},i} &= \Psi(\mathbf{E}_i) v_i \phi, \\ \phi &= \frac{V}{\sum_{j=1}^{N} v_j}, \end{aligned} \tag{4}$$

where $v_i$ represents the van der Waals volume of the atom $i$, and $\phi$ is a scaling factor that depends on the van der Waals volume of the whole protein $V$ and the sum of volumes of the $N$ atoms considered in the analysis. The scaling factor $\phi$ is especially useful for adjusting the elastic energy definition to different choices of atoms (only $C_\alpha$, main chain, all atoms, etc).

**Data import.** The Cryo-EM structures used in this study (PDB entries 7PBR, 7PBL, 7PBM, 7PBN, 7PBO, and 7PBP) were previously obtained and refined from the same experimental dataset [2]. See further details, such as structure labelling, data processing, and protein volume estimation in *SI:* Appendix A.

**Cycle reconstruction.** We start our analyses by applying PSA to evaluate the mechanical relationship among all RuvB subunits. In brief, we use strain as a measure of dissimilarity between two conformations. To this end, the strain is computed for 900 pairs of structures ($30 \times 30$) corresponding to the five hexamers in the

mechanochemical cycle ($s_1, \ldots, s_5$). The labelling of subunits was systematically shifted from one to five times so that all pairwise comparisons could be tested (for example the pair F1/D1 requires the labels to be shifted by two positions). See *SI:* Appendix B for implementation details.

Once the 900 pairwise comparisons were performed, we composed a pairwise strain matrix $M$, whose elements were defined as the mean strain $\langle \epsilon_3 \rangle$ over all the $N$ atoms considered in the analysis, $\langle \epsilon_3 \rangle = \sum_i^N \epsilon_{i,3}/N$. Because the matrix $M$ is not necessarily symmetric, we symmetrised $M$ as $\frac{1}{2}(M + M^{\mathrm{T}})$ to serve as a dissimilarity matrix for MDS, see *SI* Fig. 9A for schematics.

The approach of MDS consists of identifying a set of coordinates in a lower dimensional space (we use two dimensions, thus, $(x, y)$) for each row of the dissimilarity matrix. Because such a method relies upon a local minimization process, the low-dimensional output is not unique. We thus repeated the same approach with 100 different random seeds and took the average coordinates $(x, y)$ after a pre-alignment. For completeness we also performed this procedure including the reference structure $s_0$, see *SI* Fig. 10.

**Elastic characterisation of RuvB mechanochemical cycle.** To perform the elastic energy calculations, we used PSA considering $s_0$ as the reference state for each pairwise comparison. Thus, each cycle conformation is compared to its cognate in the reference structure, e.g., the reference for conformation F1 is F0, for F2 is F0, and so on.

Additionally, we used in PSA a neighbourhood selection method that establishes a common list of neighbouring atoms regardless of the structural comparison. For a complete description of the parameters we used, see *SI:* Appendix C. We also evaluated how different parameter choices affects the energy landscape of RuvB's cycle, showing a small impact on the overall trend *SI* Fig. 17.

**Computing polar interactions.** We identified the polar interactions of each atom using a script adapted from pymol [81] core functions, `show_contacts()`. We computed all inter and intramolecular H-bonds and optimal polar interactions (cutoff 3.5 Å) and suboptimal polar interactions (cutoff 3.9 Å). To calculate the total elastic energy of intermolecular interactions, we sum the elastic energy of all interacting residues weighted by the fraction of such interactions established with that particular molecule, see *SI* Fig. 13 for an example.

**Multiple sequence alignment and conservation.** The details are given in *SI:* Appendix E.

**Stochastic kinetic model of RuvB assembly.** Consider a system with $M$ molecules, labelled $m \in \{1, 2, \ldots, M\}$, representing each of the RuvB subunits. These molecules populate a discrete and ordered set of states, representing the protein conformations, $i \in \{1, 2, \ldots, N\}$. For the RuvB cycle, $M = 6$ and $N = 30$. Transitions in this system are caused by random interactions with a thermal reservoir of temperature $T$, inducing a molecule $m$ in state $i$ to change to one of the neighbour states ($i + 1$ or $i - 1$). We set periodic boundary conditions, allowing transitions between states 1 and $N$. We assume that a transition changes the state of a single molecule at a time.

Each of the $N$ states is associated with a reaction coordinate $\theta(i) = 2\pi i/N$. To simplify our notation, we denote as $\theta_m$ the reaction coordinate of the subunit $m$. In our analyses, we assume that these reaction coordinates correspond to the conformations observed in RuvB's mechanochemical cycle, $\theta(1) \to$ F1, $\theta(2) \to$ F2, $\ldots$, $\theta(30) \to$ A5. Thus, a hexameric assembly state can be fully described by a vector with the reaction coordinates of each subunit, for instance, $\mathbf{a} = \big[\theta_1(4), \quad \theta_2(9), \quad \theta_3(14), \quad \theta_4(18), \quad \theta_5(24), \quad \theta_6(29)\big]$ corresponds to the assembly shown in *SI* Fig. 18A.

The internal energy of the whole assembly can be decomposed in two terms. First, each state is characterised by a potential elastic energy $E_{\mathrm{el}}(\theta)$. Second, a coupling energy $E_{\mathrm{c}}$ links pairs of molecules with consecutive indices, see Fig. 7A. We define the coupling energy inspired by the Kuramoto model [82], a classical mathematical model for describing synchronous oscillators:

$$E_{\mathrm{c}}(\theta_m, \theta_{m+1}) = \frac{K}{M}\big(1 - \cos(\theta_{m+1} - \theta_m - \delta)\big) \quad , \tag{5}$$

where $K$ and $\delta$ respectively represent the coupling strength and the phase in reaction coordinate between consecutive molecules at equilibrium. The energy of the assembly can be thus summarised as

$$E(\boldsymbol{\theta}) = \sum_{m=1}^{M} E_{\mathrm{el}}(\theta_m) + E_{\mathrm{c}}(\theta_m, \theta_{m+1}) \quad . \tag{6}$$

The energetics and dynamics of the system are connected by local detailed-balance (*SI* Fig. 18B), which links transition rates between pairs of states and their respective energy difference [20]. As we mentioned previously, transitions are allowed between assembly states for which one of the molecules $m$ changes to a neighbouring state. From the allowed transitions, a few have an additional energetic contribution $\Delta\mu$, representing the external chemical drive coming from the ATP cycle. We set the kinetic rates between two arbitrary neighbouring states $\mathbf{a} = \boldsymbol{\theta}$ and $\mathbf{b} = \boldsymbol{\theta}'$ as such:

$$k_{ab} = \begin{cases} {\tau_{ab}}^{-1}\Gamma_{ab} & \text{if } \mathbf{a} \leftrightarrow \mathbf{b} \text{ is not driven} \\ {\tau_{ab}}^{-1}\Gamma_{ab}\exp\left(\frac{\Delta\mu}{2kT}\right) & \text{if } \mathbf{a} \to \mathbf{b} \text{ is driven} \\ {\tau_{ab}}^{-1}\Gamma_{ab}\exp\left(\frac{-\Delta\mu}{2kT}\right) & \text{if } \mathbf{a} \leftarrow \mathbf{b} \text{ is driven,} \end{cases} \tag{7}$$

with $\Gamma_{ab} = \big(1 + \exp((E(\mathbf{b}) - E(\mathbf{a}))/kT)\big)^{-1}$, $k$ the Boltzmann constant, and $\tau_{ab}$ the characteristic time scale

of the transition (note that $\tau_{ab} = \tau_{ba}$). See the *SI:* Appendix F for a complete description of how $\tau_{ab}$ is defined.

We simulated stochastic trajectories based on this kinetic model using the Gillespie algorithm [83].

**Model parameters and data analysis.** The details are given in *SI:* Appendix G.

**Definition of coupling energy and force per state** The details are given in *SI:* Appendix H.

**Acknowledgments**

*Acknowledgements.* P.S. and V.H.M. would like to thank J. Howard for illuminating discussions. All authors thank W. Lugmayr for discussions concerning PSA implementation. This work was financially supported by the fellowship from Fundação para a Ciência e Tecnologia (UI/BD/152254/2021) to V.H.M. and a laCaixa grant (LCF/BQ/PI21/11830032) to PS.

[1] C. Puchades, C. R. Sandate, and G. C. Lander, "The molecular principles governing the activity and functional diversity of AAA+ proteins," *Nature Reviews Molecular Cell Biology*, vol. 21, no. 1, pp. 43–58, 2020.

[2] J. Wald, D. Fahrenkamp, N. Goessweiner-Mohr, W. Lugmayr, L. Ciccarelli, O. Vesper, and T. C. Marlovits, "Mechanism of AAA+ ATPase-mediated RuvAB–Holliday junction branch migration," *Nature*, vol. 609, no. 7927, pp. 630–639, 2022.

[3] A. H. de la Peña, E. A. Goodall, S. N. Gates, G. C. Lander, and A. Martin, "Substrate-engaged 26S proteasome structures reveal mechanisms for ATP-hydrolysis–driven translocation," *Science*, vol. 362, no. 6418, p. eaav0725, 2018.

[4] M. Shin, E. R. Watson, A. S. Song, J. T. Mindrebo, S. J. Novick, P. R. Griffin, R. L. Wiseman, and G. C. Lander, "Structures of the human LONP1 protease reveal regulatory steps involved in protease activation," *Nature Communications*, vol. 12, no. 1, p. 3239, 2021.

[5] E. Zehr, A. Szyk, G. Piszczek, E. Szczesna, X. Zuo, and A. Roll-Mecak, "Katanin spiral and ring structures shed light on power stroke for microtubule severing," *Nature Structural Molecular Biology*, vol. 24, no. 9, pp. 717–725, 2017.

[6] H. Han, H. L. Schubert, J. McCullough, N. Monroe, M. D. Purdy, M. Yeager, W. I. Sundquist, and C. P. Hill, "Structure of spastin bound to a glutamate-rich peptide implies a hand-over-hand mechanism of substrate translocation," *Journal of Biological Chemistry*, vol. 295, no. 2, pp. 435–443, 2020.

[7] M. Shin, C. Puchades, A. Asmita, N. Puri, E. Adjei, R. L. Wiseman, A. W. Karzai, and G. C. Lander, "Structural basis for distinct operational modes and protease activation in AAA+ protease Lon," *Science Advances*, vol. 6, no. 21, p. eaba8404, 2020.

[8] S. N. Gates, A. L. Yokom, J. Lin, M. E. Jackrel, A. N. Rizo, N. M. Kendsersky, C. E. Buell, E. A. Sweeny, K. L. Mack, E. Chuang, M. P. Torrente, M. Su, J. Shorter, and D. R. Southworth, "Ratchet-like polypeptide translocation mechanism of the AAA+ disaggregase Hsp104," *Science*, vol. 357, no. 6348, pp. 273–279, 2017.

[9] C. Puchades, B. Ding, A. Song, R. L. Wiseman, G. C. Lander, and S. E. Glynn, "Unique Structural Features of the Mitochondrial AAA+ Protease AFG3L2 Reveal the Molecular Basis for Activity in Health and Disease," *Molecular Cell*, vol. 75, no. 5, pp. 1073–1085.e6, 2019.

[10] C. Puchades, A. J. Rampello, M. Shin, C. J. Giuliano, R. L. Wiseman, S. E. Glynn, and G. C. Lander, "Structure of the mitochondrial inner membrane AAA+ protease YME1 gives insight into substrate processing," *Science*, vol. 358, no. 6363, p. eaao0464, 2017.

[11] C. Deville, M. Carroni, K. B. Franke, M. Topf, B. Bukau, A. Mogk, and H. R. Saibil, "Structural pathway of regulated substrate transfer and threading through an Hsp100 disaggregase," *Science Advances*, vol. 3, no. 8, p. e1701726, 2017.

[12] K. I. White, M. Zhao, U. B. Choi, R. A. Pfuetzner, and A. T. Brunger, "Structural principles of SNARE complex recognition by the AAA+ protein NSF," *eLife*, vol. 7, p. e38888, 2018.

[13] C. Alfieri, L. Chang, and D. Barford, "Mechanism for remodelling of the cell cycle checkpoint protein MAD2 by the ATPase TRIP13," *Nature*, vol. 559, no. 7713, pp. 274–278, 2018.

[14] K. E. Lopez, A. N. Rizo, E. Tse, J. Lin, N. W. Scull, A. C. Thwin, A. L. Lucius, J. Shorter, and D. R. Southworth, "Conformational plasticity of the ClpAP AAA+ protease couples protein unfolding and proteolysis," *Nature Structural Molecular Biology*, vol. 27, no. 5, pp. 406–416, 2020.

[15] F. Jülicher and J. Prost, "Cooperative molecular motors," *Physical review letters*, vol. 75, no. 13, p. 2618, 1995.

[16] J.-C. Liao, Y.-J. Jeong, D.-E. Kim, S. S. Patel, and G. Oster, "Mechanochemistry of T7 DNA Helicase," *Journal of Molecular Biology*, vol. 350, no. 3, pp. 452–475, 2005.

[17] S. Liu, G. Chistol, and C. Bustamante, "Mechanical Operation and Intersubunit Coordination of Ring-Shaped Molecular Motors: Insights from Single-Molecule Studies," *Biophysical Journal*, vol. 106, no. 9, pp. 1844–1858, 2014.

[18] Y. Cao, H. Wang, Q. Ouyang, and Y. Tu, "The free-energy cost of accurate biochemical oscillations," *Nature Physics*, vol. 11, no. 9, pp. 772–778, 2015.

[19] E. Lathouwers, J. N. E. Lucero, and D. A. Sivak, "Nonequilibrium energy transduction in stochastic strongly coupled rotary motors," *The Journal of Physical Chemistry Letters*, vol. 11, no. 13, pp. 5273–5278, 2020.

[20] T. L. Hill, *Free energy transduction and biochemical cycle kinetics.* Courier Corporation, 2013.

[21] D. C. Rees and J. B. Howard, "Structural bioenergetics and energy transduction mechanisms," *Journal of Molecular Biology*, vol. 293, no. 2, pp. 343–350, 1999.

[22] A. I. Brown and D. A. Sivak, "Theory of Nonequilibrium Free Energy Transduction by Molecular Machines," *Chemical Reviews*, vol. 120, pp. 434–459, jan 2020.

[23] M. R. Mitchell, T. Tlusty, and S. Leibler, "Strain analysis of protein structures and low dimensionality of me-

chanical allosteric couplings," *Proceedings of the National Academy of Sciences*, vol. 113, no. 40, pp. E5847—-E5855, 2016.

[24] P. Sartori and S. Leibler, "Evolutionary conservation of mechanical strain distributions in functional transitions of protein structures," *Physical Review X*, vol. 14, no. 1, p. 11042, 2024.

[25] J. Howard, *Mechanics of Motor Proteins and the Cytoskeleton*. Sunderland, MA: Sinauer, 1 ed., 2001.

[26] K. Kawaguchi and S. Ishiwata, "Nucleotide-Dependent Single- to Double-Headed Binding of Kinesin," *Science*, vol. 291, no. 5504, pp. 667–669, 2001.

[27] C. Cecconi, E. A. Shank, C. Bustamante, and S. Marqusee, "Direct Observation of the Three-State Folding of a Single Protein Molecule," *Science*, vol. 309, no. 5743, pp. 2057–2060, 2005.

[28] Y. Wang and G. Zocchi, "The folded protein as a viscoelastic solid," *Europhysics Letters*, vol. 96, no. 1, p. 18003, 2011.

[29] G. M. Alushin, G. C. Lander, E. H. Kellogg, R. Zhang, D. Baker, and E. Nogales, "High-resolution microtubule structures reveal the structural transitions in $\alpha\beta$-tubulin upon GTP hydrolysis," *Cell*, vol. 157, no. 5, pp. 1117–1129, 2014.

[30] J.-H. Ha and S. N. Loh, "Protein Conformational Switches: From Nature to Design," *Chemistry – A European Journal*, vol. 18, no. 26, pp. 7984–7999, 2012.

[31] O. Keskin, S. R. Durell, I. Bahar, R. L. Jernigan, and D. G. Covell, "Relating Molecular Flexibility to Function: A Case Study of Tubulin," *Biophysical Journal*, vol. 83, pp. 663–680, aug 2002.

[32] S. Maki-Yonekura, K. Yonekura, and K. Namba, "Conformational change of flagellin for polymorphic supercoiling of the flagellar filament," *Nature Structural Molecular Biology*, vol. 17, no. 4, pp. 417–422, 2010.

[33] E. D. Zhong, T. Bepler, B. Berger, and J. H. Davis, "CryoDRGN: reconstruction of heterogeneous cryo-EM structures using neural networks.," *Nature methods*, vol. 18, pp. 176–185, feb 2021.

[34] A. J. M. Spencer, *Continuum mechanics*. Courier Corporation, 2004.

[35] W. S. Torgerson, "Multidimensional scaling: I. Theory and method," *Psychometrika*, vol. 17, no. 4, pp. 401–419, 1952.

[36] N. Saeed, H. Nam, M. I. U. Haq, and D. B. Muhammad Saqib, "A Survey on Multidimensional Scaling," *ACM Comput. Surv.*, vol. 51, no. 3, 2018.

[37] A. F. Neuwald, L. Aravind, J. L. Spouge, and E. V. Koonin, "AAA+: A class of chaperone-like ATPases associated with the assembly, operation, and disassembly of protein complexes," *Genome research*, vol. 9, no. 1, pp. 27–43, 1999.

[38] G. J. Steel, C. Harley, A. Boyd, and A. Morgan, "A screen for dominant negative mutants of SEC18 reveals a role for the AAA protein consensus sequence in ATP hydrolysis," *Molecular biology of the cell*, vol. 11, no. 4, pp. 1345–1356, 2000.

[39] D. A. Hattendorf and S. L. Lindquist, "Cooperative kinetics of both Hsp104 ATPase domains and interdomain communication revealed by AAA sensor-1 mutants," *The EMBO journal*, vol. 21, no. 1-2, pp. 12–21, 2002.

[40] T. V. Seraphim and W. A. Houry, "AAA+ proteins," *Current Biology*, vol. 30, no. 6, pp. R251—-R257, 2020.

[41] M. Jessop, J. Felix, and I. Gutsche, "AAA+ ATPases: structural insertions under the magnifying glass," *Current Opinion in Structural Biology*, vol. 66, pp. 119–128, 2021.

[42] Y.-W. Han, H. Iwasaki, T. Miyata, K. Mayanagi, K. Yamada, K. Morikawa, and H. Shinagawa, "A unique $\beta$-hairpin protruding from AAA+ ATPase domain of RuvB motor protein is involved in the interaction with RuvA DNA recognition protein for branch migration of Holliday junctions," *Journal of Biological Chemistry*, vol. 276, no. 37, pp. 35024–35028, 2001.

[43] D. Pal and P. Chakrabarti, "On residues in the disallowed region of the Ramachandran map," *Biopolymers*, vol. 63, no. 3, pp. 195–206, 2002.

[44] A. V. Finkelstein and O. Ptitsyn, *Protein physics: a course of lectures*. Elsevier, 2016.

[45] Y.-W. Han, T. Tani, M. Hayashi, T. Hishida, H. Iwasaki, H. Shinagawa, and Y. Harada, "Direct observation of DNA rotation during branch migration of Holliday junction DNA by Escherichia coli RuvA–RuvB protein complex," *Proceedings of the National Academy of Sciences*, vol. 103, no. 31, pp. 11544–11548, 2006.

[46] F. Jülicher, A. Ajdari, and J. Prost, "Modeling molecular motors," *Reviews of Modern Physics*, vol. 69, no. 4, p. 1269, 1997.

[47] D. Keller and C. Bustamante, "The Mechanochemistry of Molecular Motors," *Biophysical Journal*, vol. 78, pp. 541–556, feb 2000.

[48] M. J. Schnitzer, K. Visscher, and S. M. Block, "Force production by single kinesin motors," *Nature Cell Biology*, vol. 2, no. 10, pp. 718–723, 2000.

[49] J. Wald and T. C. Marlovits, "Holliday junction branch migration driven by AAA+ ATPase motors," *Current Opinion in Structural Biology*, vol. 82, p. 102650, 2023.

[50] R. J. D. Miller, "Energetics and Dynamics of Deterministic Protein Motion," *Accounts of Chemical Research*, vol. 27, pp. 145–150, may 1994.

[51] T. Yamato, "Strain tensor field in proteins.," *Journal of molecular graphics*, vol. 14, pp. 98–99,105–107, apr 1996.

[52] K. Koike, K. Kawaguchi, and T. Yamato, "Stress tensor analysis of the protein quake of photoactive yellow protein," *Phys. Chem. Chem. Phys.*, vol. 10, no. 10, pp. 1400–1405, 2008.

[53] M. J. Reynolds, C. Hachicho, A. G. Carl, R. Gong, and G. M. Alushin, "Bending forces and nucleotide state jointly regulate F-actin structure," *Nature*, vol. 611, no. 7935, pp. 380–386, 2022.

[54] A. Yu, E. M. Y. Lee, J. A. G. Briggs, B. K. Ganser-Pornillos, O. Pornillos, and G. A. Voth, "Strain and rupture of HIV-1 capsids during uncoating," *Proceedings of the National Academy of Sciences*, vol. 119, no. 10, p. e2117781119, 2022.

[55] J. M. McBride, K. Polev, A. Abdirasulov, V. Reinharz, B. A. Grzybowski, and T. Tlusty, "AlphaFold2 Can Predict Single-Mutation Effects," *Phys. Rev. Lett.*, vol. 131, p. 218401, nov 2023.

[56] A. Bakan and I. Bahar, "The intrinsic dynamics of enzymes plays a dominant role in determining the structural changes induced upon inhibitor binding," *Proceedings of the National Academy of Sciences*, vol. 106, no. 34, pp. 14349–14354, 2009.

[57] L. Skjærven, X.-Q. Yao, G. Scarabelli, and B. J. Grant, "Integrating protein structural dynamics and evolutionary analysis with Bio3D," *BMC Bioinformatics*, vol. 15, no. 1, p. 399, 2014.

[58] X.-Q. Yao, L. Skjærven, and B. J. Grant, "Rapid Characterization of Allosteric Networks with Ensemble Normal Mode Analysis," *The Journal of Physical Chemistry B*, vol. 120, pp. 8276–8288, aug 2016.

[59] V. Lombard, S. Grudinin, and E. Laine, "Explaining Conformational Diversity in Protein Families through Molecular Motions," *Scientific Data*, vol. 11, no. 1, p. 752, 2024.

[60] J. Frank and A. Ourmazd, "Continuous changes in structure mapped by manifold embedding of single-particle data in cryo-EM," *Methods*, vol. 100, pp. 61–67, 2016.

[61] W. S. Tang, E. D. Zhong, S. M. Hanson, E. H. Thiede, and P. Cossio, "Conformational heterogeneity and probability distributions from single-particle cryo-electron microscopy," *Current Opinion in Structural Biology*, vol. 81, p. 102626, 2023.

[62] A. Dashti, P. Schwander, R. Langlois, R. Fung, W. Li, A. Hosseinizadeh, H. Y. Liao, J. Pallesen, G. Sharma, V. A. Stupina, and Others, "Trajectories of the ribosome as a Brownian nanomachine," *Proceedings of the National Academy of Sciences*, vol. 111, no. 49, pp. 17492–17497, 2014.

[63] A. Dashti, G. Mashayekhi, M. Shekhar, D. Ben Hail, S. Salah, P. Schwander, A. des Georges, A. Singharoy, J. Frank, and A. Ourmazd, "Retrieving functional pathways of biomolecules from single-particle snapshots.," *Nature communications*, vol. 11, p. 4734, sep 2020.

[64] J. Giraldo-Barreto, S. Ortiz, E. H. Thiede, K. Palacio-Rodriguez, B. Carpenter, A. H. Barnett, and P. Cossio, "A Bayesian approach to extracting free-energy profiles from cryo-electron microscopy experiments," *Scientific Reports*, vol. 11, no. 1, p. 13657, 2021.

[65] R. G. Viegas, I. B. S. Martins, M. N. Sanches, A. B. Oliveira Junior, J. B. de Camargo, F. V. Paulovich, and V. B. P. Leite, "ELViM: Exploring Biomolecular Energy Landscapes through Multidimensional Visualization," *Journal of Chemical Information and Modeling*, vol. 64, pp. 3443–3450, apr 2024.

[66] R. Afrin, M. T. Alam, and A. Ikai, "Pretransition and progressive softening of bovine carbonic anhydrase II as probed by single molecule atomic force microscopy," *Protein science*, vol. 14, no. 6, pp. 1447–1457, 2005.

[67] M. Dong, S. Husale, and O. Sahin, "Determination of protein structural flexibility by microsecond force spectroscopy," *Nature Nanotechnology*, vol. 4, no. 8, pp. 514–517, 2009.

[68] G. Song, "Bridging between material properties of proteins and the underlying molecular interactions," *PLOS ONE*, vol. 16, no. 5, pp. 1–20, 2021.

[69] M. Krieg, A. R. Dunn, and M. B. Goodman, "Mechanical control of the sense of touch by $\beta$-spectrin," *Nature Cell Biology*, vol. 16, no. 3, pp. 224–233, 2014.

[70] E. Efrati, E. Sharon, and R. Kupferman, "The metric description of elasticity in residually stressed soft materials," *Soft Matter*, vol. 9, no. 34, pp. 8187–8197, 2013.

[71] R. G. Wolcott and P. D. Boyer, "The reversal of the myosin and actomyosin ATPase reactions and the free energy of ATP binding to myosin," *Biochemical and Biophysical Research Communications*, vol. 57, no. 3, pp. 709–716, 1974.

[72] R. Yasuda, H. Noji, M. Yoshida, K. Kinosita, and H. Itoh, "Resolution of distinct rotational substeps by submillisecond kinetic analysis of F1-ATPase," *Nature*, vol. 410, no. 6831, pp. 898–904, 2001.

[73] M. Dittrich, S. Hayashi, and K. Schulten, "On the Mechanism of ATP Hydrolysis in F1-ATPase," *Biophysical Journal*, vol. 85, no. 4, pp. 2253–2266, 2003.

[74] X. Fei, T. A. Bell, S. Jenni, B. M. Stinson, T. A. Baker, S. C. Harrison, and R. T. Sauer, "Structures of the ATP-fueled ClpXP proteolytic machine bound to protein substrate," *eLife*, vol. 9, p. e52774, 2020.

[75] V. Solanki, S. Kapoor, and K. G. Thakur, "Structural insights into the mechanism of Type IVa pilus extension and retraction ATPase motors," *The FEBS Journal*, vol. 285, no. 18, pp. 3402–3421, 2018.

[76] P. M. Gullett, M. F. Horstemeyer, M. I. Baskes, and H. Fang, "A deformation gradient tensor and strain tensors for atomistic simulations," *Modelling and Simulation in Materials Science and Engineering*, vol. 16, no. 1, p. 15001, 2007.

[77] G. A. Holzapfel, "Nonlinear solid mechanics: a continuum approach for engineering science," 2002.

[78] M. Radmacher, M. Fritz, J. P. Cleveland, D. A. Walters, and P. K. Hansma, "Imaging adhesion forces and elasticity of lysozyme adsorbed on mica with the atomic force microscope," *Langmuir*, vol. 10, no. 10, pp. 3809–3814, 1994.

[79] M. Guthold, W. Liu, E. A. Sparks, L. M. Jawerth, L. Peng, M. Falvo, R. Superfine, R. R. Hantgan, and S. T. Lord, "A comparison of the mechanical and structural properties of fibrin fibers with other protein fibers," *Cell biochemistry and biophysics*, vol. 49, pp. 165–181, 2007.

[80] H. J. Lessen, P. J. Fleming, K. G. Fleming, and A. J. Sodt, "Building blocks of the outer membrane: calculating a general elastic energy model for $\beta$-barrel membrane proteins," *Journal of chemical theory and computation*, vol. 14, no. 8, pp. 4487–4497, 2018.

[81] Schrödinger, LLC, "The PyMOL Molecular Graphics System, Version∼1.8." 2015.

[82] Y. Kuramoto, "Self-entrainment of a population of coupled non-linear oscillators," in *International Symposium on Mathematical Problems in Theoretical Physics: January 23–29, 1975, Kyoto University, Kyoto/Japan*, pp. 420–422, Springer, 1975.

[83] D. T. Gillespie, "A general method for numerically simulating the stochastic time evolution of coupled chemical reactions," *Journal of Computational Physics*, vol. 22, no. 4, pp. 403–434, 1976.

[84] C. R. Chen and G. I. Makhatadze, "ProteinVolume: calculating molecular van der Waals and void volumes in proteins," *BMC Bioinformatics*, vol. 16, no. 1, p. 101, 2015.

[85] H. Iwasaki, Y.-W. Han, T. Okamoto, T. Ohnishi, M. Yoshikawa, K. Yamada, H. Toh, H. Daiyasu, T. Ogura, and H. Shinagawa, "Mutational analysis of the functional motifs of RuvB, an AAA+ class helicase and motor protein for holliday junction branch migration," *Molecular microbiology*, vol. 36, no. 3, pp. 528–538, 2000.

[86] S. Kumar, G. Stecher, and K. Tamura, "MEGA7: Molecular Evolutionary Genetics Analysis Version 7.0 for Bigger Datasets.," *Molecular biology and evolution*, vol. 33, pp. 1870–1874, jul 2016.